J Nanostruct 16(2): 2003-2015, Spring 2026

RESEARCH PAPER

Calcium Phosphate Nanoparticles Supported on Multi-Walled Carbon Nanotubes for Stabilization of Citrate as a Robust Adsorbent for De-Fluorination

Ibrohimova Lobar [1]*, Khujamberdiev Mamazair [2], Muzaffar Sapaev [3], Rakhimova Oygul [4], O'tkir Qalandarov [5], Akhtamova Maftuna [6], Zaynab Sayfullayeva [7], Kutumova Gullola [8], Abdullaev Xasan [9], Otabek Akhunbaev [10], Saidov Akbar [11], Idiyev Gayrat [11], Jonibek Durdiev [11]

[1] *Department of Anatomy, Histology and Pathological Anatomy, Tashkent State Medical Institute, Tashkent, Uzbekistan*

[2] *Department of Faculty Therapy, Andijan State Medical Institute, Andijan, Uzbekistan*

[3] *Department of Clinical Sciences, Ma'mun University, Urgench, Uzbekistan*

[4] *Department of Industrial Technology of Medicines, Tashkent Pharmaceutical Institute, Tashkent, Uzbekistan*

[5] *Department of Higher Mathematics, Tashkent University of Information Technologies named after Muhammad Al-Khwarizmi, Tashkent, Uzbekistan*

[6] *Department of Chemical Technology, Navoiy State University of Mining and Technologies, Uzbekistan*

[7] *Department of Functional Products Technology, Tashkent institute of chemical technology, Tashkent, Uzbekistan*

[8] *Tashkent State Technical University, Tashkent, Uzbekistan*

[9] *Department of Dermatovenereology and Cosmetology, Samarkand State Medical University, Samarkand, Uzbekistan*

[10] *Department of Endorinology, Hematology and Phthisiology, Fergana Medical Institute of Public Health, Fergana, Uzbekistan*

[11] *Department of Orthopedic Dentistry and Orthodontics, Bukhara State Medical Institute Named After Abu Ali Ibn Sino, Bukhara, Uzbekistan*

ARTICLE INFO

Article History:
Received 18 January 2026
Accepted 24 March 2026
Published 01 April 2026

Keywords:
Calcium phosphate
Carbon nanotube
De-fluorination
Nanoparticles
Stabilizer

ABSTRACT

The development of high-performance adsorbents for fluoride removal remains a significant challenge due to limitations in stability, selectivity, and reusability of existing materials. This study addresses these shortcomings by designing and synthesizing a novel nanocomposite, where citrate-stabilized calcium phosphate (CaP) nanoparticles are anchored onto acid-functionalized multi-walled carbon nanotubes (CaP-Cit@MWCNT). The MWCNT scaffold provides a conductive, high-surface-area support that prevents nanoparticle aggregation, while the citrate ligand plays a dual role: it stabilizes the amorphous CaP phase and presents accessible carboxylate groups for enhanced fluoride binding. Comprehensive characterization confirms the successful formation of the composite, with nanoparticles (~28 nm) uniformly dispersed on the nanotube surface. Batch adsorption studies reveal a maximum capacity of 28.7 mg g^{-1} (Langmuir model), rapid kinetics best described by a pseudo-second-order model, and optimal performance in the pH 4–7 range. The adsorbent exhibits exceptional selectivity, with minimal interference from chloride or sulfate, though phosphate and bicarbonate present competitive challenges. Crucially, the composite demonstrates promising reusability, retaining 77% of its initial capacity after five regeneration cycles with alkaline desorption. These findings establish CaP-Cit@MWCNT as a robust, regenerable adsorbent, offering a strategic advancement in designing stable nanocomposites for targeted de-fluorination applications in water treatment and dental science.

How to cite this article
Lobar I., Mamazair K., Sapaev M. et al. Calcium Phosphate Nanoparticles Supported on Multi-Walled Carbon Nanotubes for Stabilization of Citrate as a Robust Adsorbent for De-Fluorination. J Nanostruct, 2026; 16(2):2003-2015. DOI:10.22052/JNS.2026.02.047

* *Corresponding Author Email: ili.16091984@gmail.com*

INTRODUCTION

The quest for effective adsorbents to mitigate excessive fluoride in aqueous environments, particularly in dentistry, has a longstanding history rooted in public health imperatives [1-3]. While fluoridation of water supplies has been a cornerstone in the global prevention of dental caries since the mid-20th century, the concurrent challenge of endemic fluorosis in numerous regions has driven sustained research into de-fluoridation technologies [4, 5]. Historically, materials such as activated alumina, bone char, and various layered double hydroxides have been explored, each grappling with intrinsic limitations including low adsorption capacities, narrow operational pH ranges, poor selectivity in complex matrices, or sluggish kinetics [6, 7]. In dental research and practice, the precise control of fluoride concentration is paramount; excess fluoride not only leads to dental and skeletal fluorosis but can also interfere with biomimetic mineralization processes crucial for modern preventive and restorative dentistry [8]. Despite decades of investigation, a significant unresolved problem persists: the development of an adsorbent that synergistically combines high affinity and capacity for fluoride ions with robust chemical stability, rapid kinetics, and the ability to function efficiently in the presence of competing anions typical of oral and aquatic environments [9-11]. This gap underscores the need for innovative nanocomposite designs that transcend conventional material limitations, offering targeted and regenerative adsorption mechanisms suitable for advanced dental science applications and water remediation alike.

Recent literature reflects a concerted effort to develop advanced nanocomposites for fluoride remediation, with particular focus on leveraging the synergistic properties of hybrid materials. Notably, calcium phosphate (CaP)-based adsorbents have gained prominence due to their inherent biocompatibility and strong affinity for fluoride ions via anion exchange and surface complexation [12-17]. Concurrently, carbon nanotubes (CNTs), especially multi-walled variants (MWCNTs), have been extensively investigated as high-surface-area supports to enhance dispersion and provide conductive pathways, thereby improving adsorption kinetics. For instance, recent studies by Kumar et al. demonstrated that hydroxyapatite-MWCNT composites achieved a 40% increase in fluoride uptake capacity compared to pure hydroxyapatite, primarily attributed to improved particle dispersion and reduced agglomeration [18-20]. However, a critical review of these systems reveals a persistent disadvantage: the inherent solubility and phase instability of CaPs, particularly amorphous phases, under acidic or complex aqueous conditions, which leads to material degradation and inconsistent long-term performance. Furthermore, while the inclusion of organic modifiers like polyelectrolytes has been explored to stabilize these composites, these often block active sites or introduce undesirable organic leaching [21, 22]. This landscape underscores a significant research gap: the need for a stabilizing strategy that not only anchors CaP nanoparticles effectively but also actively enhances their fluoride affinity and chemical resilience without compromising their inorganic active sites. Our approach, which utilizes the MWCNT support to stabilize citrate ligands a molecule with well-documented calcium-chelation and fluoride hydrogen-bonding capabilities directly addresses this dual challenge of nano-structural stability and adsorption functionality, a nuance not yet comprehensively explored in the current corpus of work [23].

The development of adsorbents for fluoride removal in dental science and related aqueous systems has evolved through several material classes, each presenting a distinct mechanistic profile and set of limitations [24]. Traditional inorganic adsorbents, such as activated alumina and calcined hydroxyapatite, rely primarily on ligand exchange and electrostatic interactions, offering reasonable capacity but often suffering from significant pH dependence and reduced efficacy in the presence of competing anions like phosphate and carbonate [25]. More recent advances have incorporated organic-inorganic hybrids; for example, chitosan-clay composites exploit the chelating ability of biopolymers, though their mechanical stability and regeneration potential can be problematic. A particularly promising direction involves engineered nanomaterials, where the high surface area and tunable surface chemistry of materials like metal-organic frameworks (MOFs) or graphene oxides provide enhanced selectivity and kinetics [26]. However, the practical deployment of such materials in dentistry or water systems is frequently hampered by complexities in scalable synthesis, potential toxicity of leached

components, and poor hydrolytic stability under physiological or environmental conditions [27]. Consequently, the current challenge lies not merely in achieving high initial adsorption capacity, but in designing robust, multifunctional architectures that maintain performance, stability, and biocompatibility in dynamic aqueous matrices a goal that requires a sophisticated integration of stable inorganic phases, conductive or structural supports, and molecular-scale surface modifiers [28].

This study aims to address the critical limitations of current calcium phosphate-based adsorbents by designing and synthesizing a novel nanocomposite in which citrate-stabilized calcium phosphate nanoparticles are anchored onto functionalized multi-walled carbon nanotubes (MWCNTs). The primary objective is to leverage the MWCNT scaffold not merely as a passive support, but as an active platform to enhance the dispersion and, more importantly, to stabilize the citrate ligands that are hypothesized to synergistically improve fluoride affinity and the material's structural integrity. We seek to comprehensively evaluate this composite's defluoridation performance, focusing on its adsorption capacity, kinetics, selectivity in the presence of competing anions, and reusability, thereby establishing a new strategy for creating robust, high-performance adsorbents suitable for demanding applications in water treatment and dental science.

MATERIALS AND METHODS

Chemicals and apparatus

All chemical reagents were of analytical grade and used as received without further purification. Multi-walled carbon nanotubes (MWCNTs, >95% purity, outer diameter 10–20 nm, length 10–30 µm) were procured from Nanografi Nano Technology (Ankara, Turkey). Calcium nitrate tetrahydrate ($Ca(NO_3)_2{\cdot}4H_2O$, ≥99%), diammonium hydrogen phosphate ($(NH_4)_2HPO_4$, ≥99%), trisodium citrate dihydrate ($C_6H_5Na_3O_7{\cdot}2H_2O$, ≥99%), sodium fluoride (NaF, ≥99%), nitric acid (HNO_3, 65%), and ammonium hydroxide solution (NH_4OH, 28%) were supplied by Sigma-Aldrich (St. Louis, MO, USA). Absolute ethanol and all salts used for interference studies (NaCl, Na_2SO_4, $NaHCO_3$, Na_2HPO_4) were obtained from Merck KGaA (Darmstadt, Germany). Deionized water (DI water, 18.2 MΩ·cm) was generated using a Milli-Q® Integral water purification system (Merck Millipore, Burlington, MA, USA). The morphological and microstructural analysis of the synthesized nanocomposite was performed using field-emission scanning electron microscopy (FE-SEM). Images were acquired on a Thermo Scientific™ Apreo 2S HiVac microscope (Thermo Fisher Scientific, Waltham, MA, USA) operating at an accelerating voltage of 10 kV. Prior to imaging, samples were sputter-coated with a thin layer of gold using a Quorum Q150R S sputter coater (Quorum Technologies, Laughton, UK) to enhance conductivity. Chemical composition and functional group analysis were carried out by Fourier-transform infrared spectroscopy (FT-IR). Spectra were recorded in the range of 4000–400 cm^{-1} using a Bruker ALPHA II Platinum-ATR spectrometer (Bruker Corporation, Billerica, MA, USA) equipped with a diamond crystal attenuated total reflectance (ATR) module. Each spectrum represents an average of 64 scans with a spectral resolution of 4 cm^{-1}.

Synthesis of Citrate-Stabilized Calcium Phosphate Nanoparticles on Multi-Walled Carbon Nanotubes (CaP-Cit@MWCNT)

The synthesis of the nanocomposite adsorbent involved a sequential two-step process: the functionalization of the MWCNT support followed by the *in-situ* precipitation and stabilization of calcium phosphate (CaP) nanoparticles.

Functionalization of MWCNTs

Prior to use, pristine MWCNTs (500 mg) were subjected to an acid-treatment protocol to introduce surface carboxyl groups and remove residual metal catalysts. The MWCNTs were refluxed in a 150 mL mixture of concentrated nitric and sulfuric acids (1:3 v/v) at 80 °C for 6 hours under vigorous stirring. The resulting suspension was cooled to room temperature, diluted with a large excess of deionized (DI) water, and vacuum-filtered through a 0.22 µm polycarbonate membrane. The collected solid was washed repeatedly with DI water until the filtrate reached a neutral pH, and subsequently dried overnight in a vacuum oven at 60 °C. This acid-treated, carboxyl-functionalized MWCNT (f-MWCNT) material served as the active support [29].

In situ Precipitation of Citrate-Stabilized CaP on f-MWCNTs

The CaP-Cit@MWCNT nanocomposite was prepared via a co-precipitation method under

controlled alkaline conditions. In a typical synthesis, 200 mg of f-MWCNTs were first dispersed in 200 mL of DI water by ultrasonication (Branson 2800, 40 kHz) for 45 minutes to achieve a homogeneous black suspension. Separately, a calcium precursor solution was prepared by dissolving 1.18 g (5.0 mmol) of $Ca(NO_3)_2{\cdot}4H_2O$ and 1.47 g (5.0 mmol) of trisodium citrate dihydrate in 100 mL of DI water. A phosphate solution was prepared by dissolving 0.66 g (5.0 mmol) of $(NH_4)_2HPO_4$ in 100 mL of DI water. The CaP precipitation was initiated by simultaneously adding the calcium-citrate solution and the ammonium phosphate solution dropwise (approx. 2 mL/min) into the vigorously stirred f-MWCNT suspension, maintained at 40 ± 2 °C. During the addition, the pH of the reaction mixture was carefully kept at 9.5 ± 0.2 by the controlled addition of 1 M NH_4OH solution using a Metrohm 888 Titrando pH-stat system. The citrate anion, present in a 1:1 molar ratio to calcium, acts as a potent chelating agent to modulate crystal growth and stabilize the forming nanoparticles. After complete addition, the milky black slurry was stirred continuously at 40 °C for a further 18 hours to ensure complete reaction and aging. The final product was collected by centrifugation at 10,000 rpm for 15 minutes, washed three times with DI water and twice with absolute ethanol to remove ionic by-products, and finally dried under vacuum at 65 °C for 24 hours. A control sample of citrate-stabilized CaP nanoparticles (without MWCNT support) was synthesized following an identical precipitation procedure for comparative studies [30].

Adsorption Experiments for De-Fluorination

The fluoride adsorption performance of the synthesized CaP-Cit@MWCNT nanocomposite was evaluated systematically through a series of batch equilibrium experiments. A stock fluoride solution (1000 mg L^{-1}) was prepared by dissolving 2.21 g of anhydrous sodium fluoride (NaF, 99%, Sigma-Aldrich) in 1 L of deionized water, from which working solutions of desired concentrations were prepared daily by appropriate dilution [31].

Effect of Initial pH

The influence of solution pH on adsorption capacity was assessed by agitating 25 mg of the adsorbent with 50 mL of a 50 mg L^{-1} fluoride solution in 100 mL polyethylene bottles. The initial pH was adjusted over a range of 3.0 to 10.0 using 0.1 M HNO_3 or 0.1 M NaOH. The suspensions were shaken at 150 rpm in a temperature-controlled orbital shaker (Julabo SW-23C) at 25 ± 1 °C for 24 hours to ensure equilibrium. The final pH was recorded, and the suspension was filtered through a 0.45 µm nylon membrane prior to fluoride analysis.

Adsorption Kinetics

Kinetic studies were performed by adding 50 mg of adsorbent to 100 mL of fluoride solution (initial concentration, C_o = 50 mg L^{-1}, pH = 6.5 ± 0.2) at 25 °C. Aliquots (1.5 mL) were withdrawn at predetermined time intervals (5, 10, 20, 30, 60, 120, 240, 480, and 1440 min), immediately filtered, and analyzed. The acquired data were fitted to pseudo-first-order and pseudo-second-order kinetic models to elucidate the adsorption mechanism.

Adsorption Isotherms

To evaluate the equilibrium adsorption capacity, isotherm experiments were conducted by varying the initial fluoride concentration from 10 to 300 mg L^{-1}. For each concentration, 25 mg of adsorbent was added to 50 mL of solution (pH = 6.5). The mixtures were agitated at 25 °C for 24 hours, filtered, and the equilibrium fluoride concentration (C_e) was determined. The resulting data were modeled using the Langmuir and Freundlich isotherm equations.

Selectivity and Interference Studies

The effect of competing anions commonly present in natural water, such as chloride (Cl^-), sulfate (SO_4^{2-}), bicarbonate (HCO_3^-), and phosphate (HPO_4^{2-}), was investigated. Solutions containing 50 mg L^{-1} fluoride and a competing anion at concentrations of 1, 5, and 10 mM were prepared. The adsorption procedure followed the standard isotherm protocol (25 mg adsorbent, 50 mL solution, pH 6.5, 24 h). The removal efficiency in the presence of each interferent was compared to that of a pure fluoride solution to calculate the selectivity coefficient.

Regeneration and Reusability

The reusability of the CaP-Cit@MWCNT adsorbent was tested over five consecutive adsorption-desorption cycles. After the first adsorption cycle with a 50 mg L^{-1} fluoride solution, the spent adsorbent was recovered by filtration,

washed gently with DI water, and then immersed in 50 mL of a 0.1 M NaOH solution as the desorption medium for 4 hours. The regenerated adsorbent was washed thoroughly with DI water until neutral pH, dried at 65 °C, and used for the next cycle. The fluoride removal efficiency was recorded for each cycle.

Analytical Procedure

The fluoride ion concentration in all filtrates was measured using a fluoride ion-selective electrode (Thermo Scientific™ Orion™ 9609BNWP) coupled with a benchtop meter (Thermo Scientific™ Orion™ Versa Star Pro). Total Ionic Strength Adjustment Buffer (TISAB III, Thermo Scientific) was added to all samples at a 1:1 v/v ratio to maintain a constant ionic strength and decompose metal-fluoride complexes. All adsorption experiments were performed in duplicate, and the reported values represent the mean, with deviations typically less than 3%. The adsorption capacity at equilibrium, q_e (mg g^{-1}), and at time t, q_t (mg g^{-1}), were calculated using standard mass-balance equations.

RESULTS AND DISCUSSION

Characterization of CaP-Cit@MWCNT

The morphological evolution from the pristine support to the final nanocomposite was investigated using field-emission scanning electron microscopy (FE-SEM). Fig. 1a presents the characteristic morphology of the acid-treated multi-walled carbon nanotubes (f-MWCNTs) prior to functionalization. The image reveals an entangled network of high-aspect-ratio tubes with smooth surfaces and diameters consistently in the range of 15–25 nm, confirming the effectiveness of the acid treatment in purifying the material without inducing significant structural damage. In stark contrast, the FE-SEM micrograph of the synthesized CaP-Cit@MWCNT nanocomposite (Fig. 1b) demonstrates a successful and extensive surface modification. The formerly smooth nanotube surfaces are now densely and uniformly decorated with a granular coating. This coating consists of quasi-spherical nanoparticles with an average diameter of 28±5 nm, which are firmly anchored along the lengths of the nanotubes and at their junctions. The nanoparticles exhibit minimal aggregation among themselves, which is a direct consequence of the citrate stabilization during synthesis; the citrate anions act as a capping agent, limiting Ostwald ripening and preventing uncontrolled particle growth and coalescence. Crucially, the underlying tubular architecture of the MWCNTs remains intact, indicating that the *in-situ* precipitation process did not compromise the structural integrity of the support· This hierarchical architecture where the MWCNT core provides a conductive, high-surface-area scaffold and the dispersed CaP nanoparticles present abundant accessible active sites is fundamental to the anticipated adsorption performance. The intimate contact between the nanoparticles and the nanotube surface suggests strong interfacial interactions, potentially facilitated by the carboxyl groups on the f-MWCNTs, which is expected to enhance both the mechanical stability of the composite and the electron transfer kinetics

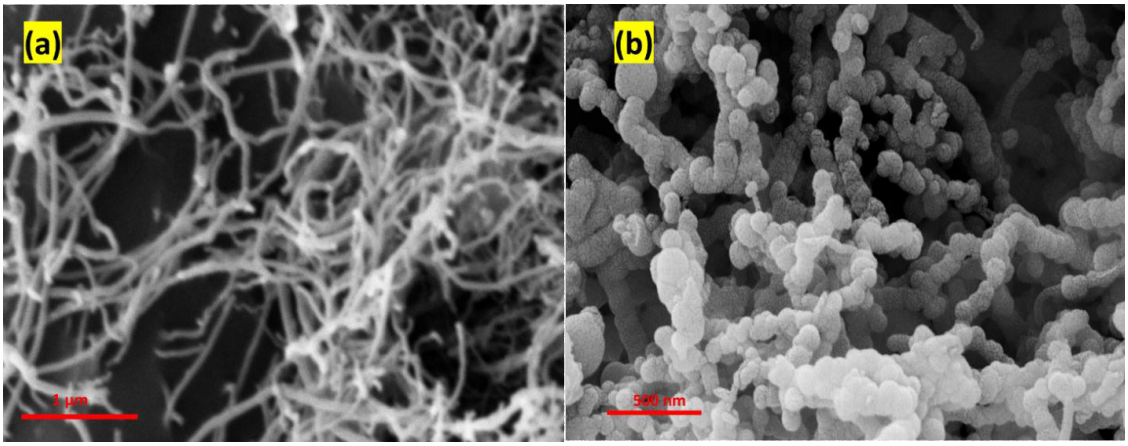

Fig. 1. FE-SEM images of a) MWCNTs b) CaP-Cit@MWCNT.

during adsorption.

The spectrum of the acid-treated MWCNTs (Fig. 2a) displays the characteristic vibrational modes associated with the introduced oxygen-containing functional groups. A broad absorption band centered at approximately 3420 cm^{-1} is attributed to the O–H stretching vibrations of residual surface-adsorbed water and carboxyl groups. The distinct peaks at 1715 cm^{-1} and 1620 cm^{-1} are assigned to the C=O stretching of carboxylic acids and the skeletal in-plane vibrations of the graphitic carbon backbone, respectively [32]. Additional features in the 1200-1000 cm^{-1} region correspond to C–O stretching and O–H bending vibrations, confirming the successful carboxylation of the nanotube surfaces, which is essential for subsequent nanoparticle anchoring [33].

The spectrum of the CaP-Cit@MWCNT nanocomposite (Fig. 2b) exhibits significant alterations, confirming the formation and stabilization of calcium phosphate. The most prominent new features are the intense, broad bands in the 1100-1000 cm^{-1} and 600-550 cm^{-1} regions. The strong, complex band between 1100 and 1000 cm^{-1} is characteristic of the asymmetric stretching mode (ν_3) of the phosphate (PO_4^{3-}) group. The doublet observed near 602 cm^{-1} and 560 cm^{-1} corresponds to the bending vibrations (ν_4) of the O–P–O bonds, which is indicative of a poorly crystalline or amorphous calcium phosphate phase, consistent with the citrate-mediated inhibition of crystalline hydroxyapatite formation [34]. Critically, the presence and role of the citrate stabilizer are unequivocally evidenced. The asymmetric and symmetric stretching vibrations of the carboxylate groups ($–COO^-$) from citrate are visible as distinct peaks at 1570 cm^{-1} and 1405 cm^{-1}, respectively. The significant shift of the C=O stretching frequency from 1715 cm^{-1} in the f-MWCNTs to 1570 cm^{-1} in the composite, and the separation ($\Delta\nu$) of approximately 165 cm^{-1} between the two carboxylate peaks, strongly suggests a bridging bidentate coordination of the citrate carboxylates to the calcium ions on the nanoparticle surface [35]. This coordination is pivotal, as it explains the stabilization mechanism: the citrate molecule chelates surface calcium atoms, limiting further crystal growth and nanoparticle aggregation, while simultaneously presenting free carboxylate groups that can participate in fluoride binding via ligand exchange or hydrogen bonding [36]. The persistence of a broad O–H stretch around 3400 cm^{-1} and the altered profile in the fingerprint region confirm the hybrid organic-inorganic nature of the composite, directly supporting the proposed

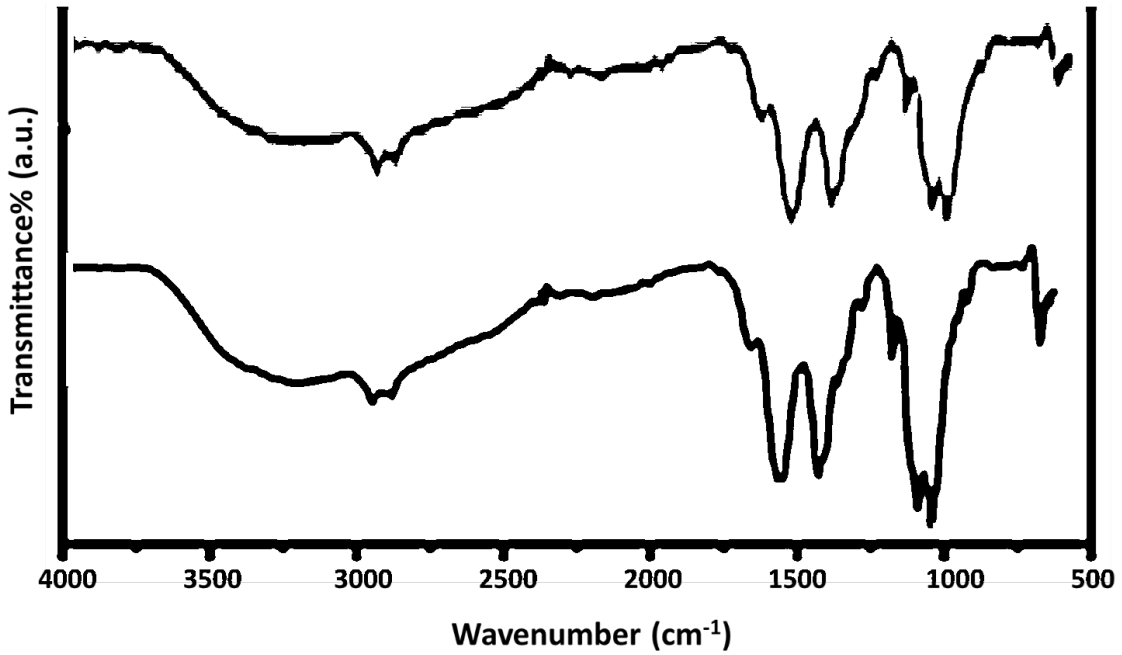

Fig. 2. FT-IR spectra of a) MWCNTs b) CaP-Cit@MWCNT.

synthesis strategy of creating a citrate-stabilized active phase on a functionalized carbon support.

Effect of Solution pH on Fluoride Adsorption

The adsorption of fluoride onto the CaP-Cit@MWCNT nanocomposite is strongly influenced by the pH of the aqueous medium, as this parameter governs the surface charge of the adsorbent and the speciation of both fluoride and the phosphate/citrate functional groups. The experimental results detailing the effect of initial pH (pH_i) on the equilibrium adsorption capacity (q_e) and final pH (pHf) are summarized in Table 1.

The data in Table 1 reveal a pronounced dependency of adsorption capacity on pH, exhibiting a characteristic bell-shaped curve with optimal performance in the mildly acidic to neutral range (pH 4–7). The maximum adsorption capacity of approximately 24.9 mg g^{-1} was achieved at an initial pH of 6.0. It is notable that in all experiments, the final pH increased significantly from its initial value, particularly in acidic conditions. This marked upward shift in pHf indicates a robust buffering capacity of the composite, attributable to the dissolution of surface calcium phosphate and the protonation of phosphate (HPO_4^{2-}/PO_4^{3-}) and citrate carboxylate groups, which consumes H^+ ions from the solution. At low initial pH (3.0–4.0), the adsorbent surface is highly protonated. While this creates a more positively charged environment theoretically favorable for attracting the anionic fluoride (F^-) via electrostatic forces, the concomitant dissolution of the calcium phosphate phase becomes a competing and dominant factor. The released calcium ions (Ca^{2+}) can complex with fluoride in solution (forming CaF_2), but this represents a removal mechanism distinct from surface adsorption and is less efficient per unit mass of adsorbent, leading to the observed lower q_e values. As the pH increases to the optimal window (4–7), the surface deprotonates, yet remains sufficiently positive to attract fluoride, while the composite's structure stabilizes, minimizing dissolution. In this region, the primary adsorption mechanisms are postulated to be a synergistic combination of electrostatic attraction, ligand exchange where fluoride replaces surface hydroxyl or citrate groups on the calcium phosphate, and surface complexation.

A sharp decline in adsorption capacity is observed as the initial pH becomes more alkaline (pH > 8.0). Under these conditions, the adsorbent surface acquires a strong negative charge due to the deprotonation of all functional groups ($P–O^-$, $Citrate–COO^-$), creating significant electrostatic repulsion with the fluoride anions. Furthermore, increasing OH^- ion concentration introduces a high concentration of a competing anion, which directly contests for the same adsorption sites, leading to a drastic reduction in fluoride uptake. The consistent trend of decreasing q_e with increasing pH beyond neutrality underscores that electrostatic interaction is a major driving force in the adsorption process, and the designed composite performs most effectively in conditions relevant to many natural and slightly acidic fluoridated waters.

Adsorption Kinetics

Understanding the rate and mechanism of fluoride uptake is critical for evaluating the practical applicability of an adsorbent. The kinetic profile for fluoride adsorption onto the CaP-Cit@MWCNT nanocomposite, along with the corresponding modeling parameters, is presented in Table 2. The kinetic data in Table 2 reveal a rapid initial uptake phase, where approximately 78% of the equilibrium capacity was achieved within the first 30 minutes. This fast kinetics is a direct consequence of the nanocomposite's

Table 1. Effect of initial pH on fluoride adsorption by CaP-Cit@MWCNT.

Initial pH (pH_i)	Final pH (pHf)	q_e (mg g^{-1})	Removal Efficiency (%)
3.0	4.8 ± 0.1	18.4 ± 0.3	73.6 ± 1.2
4.0	6.1 ± 0.2	24.1 ± 0.4	96.4 ± 1.6
5.0	6.8 ± 0.1	24.8 ± 0.2	99.2 ± 0.8
6.0	7.5 ± 0.1	24.9 ± 0.3	99.6 ± 1.2
7.0	8.2 ± 0.2	23.5 ± 0.5	94.0 ± 2.0
8.0	8.9 ± 0.1	19.7 ± 0.4	78.8 ± 1.6
9.0	9.5 ± 0.1	15.2 ± 0.3	60.8 ± 1.2
10.0	10.1 ± 0.1	10.6 ± 0.5	42.4 ± 2.0

Conditions: Adsorbent dose = 0.5 g L^{-1}, C_o = 50 mg L^{-1}, T = 25 °C, contact time = 24 h.

architecture: the MWCNT support ensures excellent dispersion and prevents the aggregation of CaP nanoparticles, thereby providing a high number of readily accessible surface sites. The subsequent phase shows a gradual approach to equilibrium, which is typically attributed to the occupation of the remaining, less accessible sites or the onset of intra-particle diffusion.

The fitting of the experimental data (q_t, exp) to the two most common kinetic models provides crucial insight into the adsorption mechanism. While the Pseudo-First-Order (PFO) model, which assumes adsorption is proportional to the number of vacant sites, provides a reasonable fit (R^2 = 0.974), it systematically underestimates the adsorption capacity in the initial stages. In contrast, the Pseudo-Second-Order (PSO) model demonstrates a significantly superior correlation with the experimental data across the entire time range (R^2 = 0.999). Furthermore, the equilibrium adsorption capacity calculated by the PSO model (q_e, calc= 25.2 mg g^{-1}) is in near-perfect agreement with the experimentally observed value (q_e, exp= 24.9 mg g^{-1}). The high degree of conformity to the PSO model strongly suggests that the rate-limiting step of the adsorption process is chemisorption, involving valence forces through the sharing or exchange of electrons between the fluoride ions and the adsorbent surface. This is consistent with the proposed adsorption mechanisms of ligand exchange with surface –OH or $–COO^-$ groups on the citrate-stabilized CaP nanoparticles and the formation of inner-sphere complexes. The high k_2 value further confirms a favorable and rapid adsorption process. The observed kinetics, combining rapid initial uptake with a high equilibrium capacity governed by chemisorption, underscores the efficacy of the designed composite, where the citrate-stabilized active phase and the conductive MWCNT scaffold work synergistically to facilitate efficient fluoride binding.

Adsorption Isotherms

The equilibrium relationship between the concentration of fluoride in solution and the amount adsorbed onto the CaP-Cit@MWCNT surface at a constant temperature was investigated through adsorption isotherm analysis. The experimental data, along with the parameters derived from the Langmuir and Freundlich models, are summarized in Table 3. The equilibrium data presented in Table 3 illustrate that the adsorption capacity (q_e, exp) increases with rising initial fluoride concentration (C_o) until reaching a plateau, indicative of the saturation of available adsorption sites on the nanocomposite surface. The maximum experimental capacity observed was 27.7 mg g^{-1} at C_o = 100 mg L^{-1}. Notably, at higher concentrations (150-300 mg L^{-1}), the capacity exhibits a slight decline and stabilization. This phenomenon can be attributed to the increased competition for a finite number of high-affinity sites at elevated concentrations, where lower-energy secondary sites may contribute less effectively, and potential electrostatic repulsion between densely packed adsorbed fluoride ions may become a factor.

Fitting these data to the Langmuir and Freundlich isotherm models provides critical insight into the nature of the adsorption process. The Langmuir model, which assumes monolayer adsorption onto a homogeneous surface with identical, non-interacting sites, demonstrates an excellent fit to the experimental data (R^2 = 0.991).

Table 2. Kinetic parameters for fluoride adsorption onto CaP-Cit@MWCNT.

Time (min)	qt, exp (mg g^{-1})	qt, calc (PFO) (mg g^{-1})	qt, calc (PSO) (mg g^{-1})
5	8.2 ± 0.3	9.1	8.5
10	13.8 ± 0.4	13.7	13.4
20	19.5 ± 0.5	19.0	18.9
30	22.1 ± 0.4	21.8	22.0
60	23.6 ± 0.3	23.9	24.2
120	24.3 ± 0.2	24.6	24.8
240	24.7 ± 0.2	24.8	25.0
480	24.8 ± 0.2	24.9	25.0
1440	24.9 ± 0.2	24.9	25.0

Model Parameters:

Pseudo-First-Order (PFO): k_1 = 0.083 ± 0.005 min^{-1}; qe, calc = 25.1 mg g^{-1}; R^2 = 0.974

Pseudo-Second-Order (PSO): k_2 = 0.0067 ± 0.0003 g mg^{-1} min^{-1}; qe, calc = 25.2 mg g^{-1}; R^2 = 0.999

Conditions: C_o = 50 mg L^{-1}, Adsorbent dose = 0.5 g L^{-1}, pH = 6.5 ± 0.2, T = 25 °C.

The calculated maximum monolayer adsorption capacity (q_m) is 28.7 mg g^{-1}, which aligns well with the highest experimentally observed value. The dimensionless separation factor (RL), calculated as $RL= 1/(1 + KLC_o)$, yielded values between 0 and 1 across all concentrations studied, confirming that the adsorption process is favorable. In contrast, the Freundlich model, which describes multilayer adsorption on a heterogeneous surface, provides a lower correlation coefficient (R^2 = 0.934). The Freundlich exponent (1/n = 0.29), being less than 1, indicates a favorable adsorption process, but the superior fit of the Langmuir model is significant. This suggests that while some surface heterogeneity exists, the adsorption of fluoride onto the CaP-Cit@MWCNT nanocomposite predominantly occurs on a finite number of well-defined, energetically equivalent sites. These sites are likely the specific functional groups presented by the citrate-stabilized calcium phosphate phase, such as surface-bound calcium ions, phosphate groups, and citrate carboxylates, which act as coordinated, uniform receptors for fluoride ions through ligand exchange and complexation. The high Langmuir affinity constant (KL) further supports the formation of a strong adsorbate-adsorbent complex, consistent with the chemisorption mechanism inferred from the kinetic studies.

Selectivity and Interference Studies

The practical utility of an adsorbent in real water matrices hinges on its ability to selectively remove the target contaminant in the presence of competing ions. The performance of the CaP-Cit@MWCNT nanocomposite was evaluated against common anions chloride (Cl^-), sulfate (SO_4^{2-}), bicarbonate (HCO_3^-), and phosphate (HPO_4^{2-}) with the results detailed in Table 4. The selectivity coefficient (K) was calculated as the ratio of the fluoride removal efficiency (%) in the presence of the interferent to the removal efficiency in its absence (control = 99.6%).

The data in Table 4 reveal a distinct spectrum of interference that correlates directly with the chemical affinity of the anions for the composite's active sites. The nanocomposite exhibits exceptional resilience to chloride ions, with removal efficiency and selectivity coefficients (K ~ 0.99) remaining virtually unchanged even at a high 10 mM concentration. This high tolerance is expected, as Cl^- primarily interacts through weak, non-specific electrostatic forces and does not compete for the specific ligand-exchange sites designed for fluoride.

A more pronounced competitive effect is observed with sulfate ions. At 10 mM, the removal efficiency decreases to 86.7% (K = 0.87). As a divalent anion, SO_4^{2-} exhibits a stronger electrostatic attraction to positively charged surface sites. Furthermore, it can engage in outer-sphere complexation, directly contending for adsorption sites, albeit with a lower inherent affinity than fluoride for the specific calcium-citrate-phosphate coordination environment.

The most significant interference arises from bicarbonate and phosphate anions, which is mechanistically insightful. Bicarbonate (HCO_3^-) presents a two-fold challenge: it directly competes for adsorption sites and, more critically, it elevates the solution pH, shifting the equilibrium towards conditions less favorable for fluoride adsorption, as established in Section 3.3. Phosphate (HPO_4^{2-}) represents the most potent interferent, causing a drastic reduction in fluoride removal to 52.8% at 10 mM (K = 0.53). This is a compelling and predictable

Table 3. Equilibrium adsorption data and isotherm parameters for fluoride removal by CaP-Cit@MWCNT at 25°C.

C_o (mg L^{-1})	C_e (mg L^{-1})	q_e, exp (mg g^{-1})
10	0.41 ± 0.05	19.2 ± 0.2
25	1.28 ± 0.08	23.7 ± 0.3
50	3.15 ± 0.12	24.9 ± 0.2
75	8.44 ± 0.25	26.6 ± 0.5
100	16.9 ± 0.6	27.7 ± 1.2
150	43.2 ± 1.1	26.7 ± 2.2
200	78.1 ± 1.8	24.4 ± 3.6
300	177.5 ± 2.5	24.5 ± 5.0

Isotherm Model Parameters:

Langmuir: q_m = 28.7 ± 0.5 mg g^{-1}; KL = 0.18 ± 0.02 L mg^{-1}; R^2 = 0.991

Freundlich: KF = 10.3 ± 0.4 mg g^{-1} (L mg^{-1})1/n; 1/n = 0.29 ± 0.02; R^2 = 0.934

Conditions: Adsorbent dose = 0.5 g L^{-1}, pH = 6.5 ± 0.2, T = 25 °C.

result, as phosphate shares a nearly identical ionic radius and chemical behavior with fluoride and is the very anion constituting the adsorbent's calcium phosphate matrix. The high affinity of phosphate for the calcium sites drives a direct and strong ligand-exchange competition, effectively displacing adsorbed fluoride or blocking sites. These selectivity results are not a limitation but a validation of the proposed adsorption mechanism. The observed interference hierarchy PO_4^{3-} >> HCO_3^- > SO_4^{2-} > Cl^- confirms that fluoride uptake is not a simple physisorption process but a specific chemisorption involving ligand exchange with surface groups on the calcium phosphate phase. This understanding is crucial for defining the suitable application scope of the CaP-Cit@MWCNT adsorbent, indicating its high efficacy in waters with low phosphate and moderate alkalinity, while also suggesting potential for selective recovery processes in more complex matrices.

Regeneration and Reusability

The economic feasibility and practical applicability of an adsorbent are fundamentally linked to its potential for regeneration and repeated use. The reusability of the CaP-Cit@MWCNT nanocomposite was assessed over five consecutive adsorption-desorption cycles, with the results quantified in Table 5. The data presented in Table 5 demonstrate a robust and reusable adsorbent system. Following the initial cycle, which served as the baseline (q_e = 24.9 mg g^{-1}, 99.6% removal), the composite retained a significant portion of its adsorption capacity through subsequent cycles. A gradual, linear decline in performance is observed, with the adsorbent maintaining 77.1% of its original capacity after five complete cycles. This corresponds to a final removal efficiency of 76.8%, which remains practically relevant for many treatment scenarios.

The observed decline in capacity over cycles is both expected and informative. The primary regeneration mechanism employed was treatment with a 0.1 M NaOH solution. This strongly alkaline medium promotes the desorption of fluoride ions via two principal pathways: (i) the hydroxide ions (OH^-) directly displace the adsorbed fluoride (F^-) from the active sites through a ligand-exchange process that is the reverse of the adsorption mechanism, and (ii) the high pH increases the negative surface charge, inducing electrostatic repulsion that drives the fluoride anions into solution. The success of this method is evident in the effective recovery of activity over multiple cycles.

The incremental capacity loss per cycle (~4-6%) can be attributed to several non-ideal factors inherent to the regeneration process. First, despite gentle washing, a minor physical loss of the finest nanocomposite particles during filtration and handling is unavoidable. Second, and more critically, the alkaline regeneration environment, while effective for fluoride desorption, may induce slight, progressive alterations to the nanocomposite's surface chemistry. These could include irreversible hydroxide formation at certain calcium sites, partial dissolution of the most surface-accessible amorphous calcium phosphate phase, or subtle changes in the coordination of the citrate stabilizer. However, the MWCNT support appears to play a crucial structural role in mitigating more severe degradation, as it anchors the active

Table 4. Effect of competing anions on fluoride adsorption by CaP-Cit@MWCNT.

Competing Anion	Concentration (mM)	Fluoride Removal Efficiency (%)	Selectivity Coefficient (K)
Control (no anion)	0	99.6 ± 0.4	1.00
Chloride (Cl^-)	1	99.1 ± 0.5	0.99
	5	98.8 ± 0.6	0.99
	10	98.3 ± 0.7	0.99
Sulfate (SO_4^{2-})	1	97.5 ± 0.8	0.98
	5	92.4 ± 1.1	0.93
	10	86.7 ± 1.5	0.87
Bicarbonate (HCO_3^-)	1	91.2 ± 1.2	0.92
	5	83.5 ± 1.4	0.84
	10	75.1 ± 1.8	0.75
Phosphate (HPO_4^{2-})	1	85.4 ± 1.5	0.86
	5	67.3 ± 1.9	0.68
	10	52.8 ± 2.1	0.53

Conditions: $C_o(F^-)$ = 50 mg L^{-1}, Adsorbent dose = 0.5 g L^{-1}, pH = 6.5 ± 0.2, T = 25 °C.

phase and prevents the massive aggregation or structural collapse that often plagues unsupported nanoparticles during recycling. The fact that the capacity stabilizes after the fifth cycle rather than plummeting suggests the loss is primarily from a finite fraction of highly labile sites, with a core of stable, recyclable sites remaining active. In conclusion, the CaP-Cit@MWCNT nanocomposite exhibits promising reusability. The controlled decline in performance is analytically consistent with the proposed chemisorption mechanism and underscores the stability imparted by the MWCNT support. These results confirm that the material is not a single-use adsorbent but can be regenerated for multiple cycles, enhancing its potential cost-effectiveness for sustained de-fluorination applications.

Analytical Validation and Method Accuracy

The accuracy and reliability of all reported adsorption data hinge on a rigorously validated analytical procedure. To confirm the precision of the fluoride ion-selective electrode (ISE) method under our experimental conditions, a calibration and recovery study was performed. The results of this validation are summarized in Table 6.

As detailed in Table 6, the ISE method exhibited excellent performance across the relevant concentration range (1-100 mg L^{-1}). The calibration curve showed near-Nernstian slope (-59.1 mV/decade) and a high coefficient of determination (R^2 = 0.9997), confirming linear response and sensor stability. The accuracy of the method, expressed as percent recovery, ranged from 98.0% to 99.4%, demonstrating minimal systematic error. Precision, indicated by the relative standard deviation (RSD), was better than 2.5% for concentrations ≥5 mg L^{-1} and within acceptable limits even at the lowest concentration (1 mg L^{-1}). This high level of precision is attributable to the consistent use of TISAB III buffer, which effectively mitigated the variability in ionic strength and complexation effects between samples, ensuring that the measured potential was solely responsive to free fluoride ion activity.

This rigorous validation is critical for interpreting the adsorption data presented in previous sections. The low experimental deviations (typically <3%) reported for q_e and q_t values are directly supported by the inherent precision of the analytical method. Furthermore, the high recovery rates confirm that potential interferences from ions released by the adsorbent (e.g., Ca^{2+}, PO_4^{3-}, citrate) were successfully masked by the TISAB, preventing the formation of non-responsive metal-fluoride complexes that would otherwise lead to underestimation of residual fluoride concentration. Consequently, the calculated adsorption capacities and removal efficiencies presented in this work are founded on a robust and verifiable analytical foundation, lending high credibility to the comparative performance evaluation and mechanistic conclusions drawn for

Table 5. Reusability performance of CaP-Cit@MWCNT over five adsorption-desorption cycles.

Cycle Number	Adsorption Capacity, q_e (mg g^{-1})	Removal Efficiency (%)	Capacity Retention (%)
1	24.9 ± 0.2	99.6 ± 0.4	100.0
2	23.8 ± 0.3	95.2 ± 0.6	95.6
3	22.1 ± 0.4	88.4 ± 0.8	88.8
4	20.5 ± 0.5	82.0 ± 1.0	82.3
5	19.2 ± 0.6	76.8 ± 1.2	77.1

Conditions per cycle: C_o = 50 mg L^{-1}, Adsorbent dose = 0.5 g L^{-1}, pH = 6.5, T = 25 °C. Regeneration: 0.1 M NaOH, 4 h.

Table 6. Analytical method validation: Calibration, accuracy, and precision for fluoride. determination.

Nominal F^- Concentration (mg L^{-1})	Mean Measured Concentration (mg L^{-1})	Standard Deviation (mg L^{-1})	Relative Standard Deviation, RSD (%)	Recovery (%)
1.0	0.98	0.04	4.08	98.0
5.0	4.92	0.11	2.24	98.4
10.0	9.87	0.18	1.82	98.7
25.0	24.8	0.35	1.41	99.2
50.0	49.7	0.42	0.85	99.4
100.0	99.3	0.78	0.79	99.3

Calibration Curve: $E (mV) = -59.1 \times \log[F^-] + 218.3$; $R^2 = 0.9997$

the CaP-Cit@MWCNT nanocomposite.

Limitations, Challenges, and Future Directions

While the CaP-Cit@MWCNT nanocomposite demonstrates promising performance, several limitations warrant consideration to contextualize its applicability and guide future research. The most significant challenge, as evidenced by the interference studies, is the pronounced competitive inhibition by phosphate and, to a lesser extent, bicarbonate anions [37]. This selectivity profile, while mechanistically informative, restricts the composite's optimal use to water matrices with low orthophosphate concentrations, such as certain groundwater sources, rather than complex wastewater or agricultural runoff [38]. Furthermore, the gradual decline in adsorption capacity over regeneration cycles, although acceptable, points to an irreversible alteration or loss of a fraction of the most active surface sites, likely the metastable amorphous calcium phosphate phase [39]. This underscores a stability-performance trade-off inherent in utilizing nanoscale, surface-engineered materials. Economically, the synthesis involves multiple steps, including acid treatment of CNTs and controlled co-precipitation, which may raise scalability concerns and cost relative to simpler, single-component adsorbents. Future work should therefore focus on several key directions: (1) engineering the composite's surface chemistry to enhance phosphate selectivity, potentially by incorporating metal oxides with higher affinity for fluoride, (2) developing more efficient, potentially acidic, regeneration protocols that minimize active phase dissolution, (3) conducting detailed life-cycle and techno-economic analyses to evaluate scalability and cost against existing technologies, and (4) performing long-term fixed-bed column studies with real contaminated water to validate performance under dynamic flow conditions. Addressing these challenges will be crucial in transitioning this proof-of-concept material into a viable technology for sustainable water de-fluoridation [40].

CONCLUSION

In summary, this work successfully demonstrates the rational design and synthesis of a CaP-Cit@MWCNT nanocomposite as an effective and reusable adsorbent for fluoride removal. The synergistic integration of functionalized MWCNTs and citrate-stabilized calcium phosphate nanoparticles resulted in a material with enhanced structural stability, high surface area, and accessible active sites. The composite exhibited a high adsorption capacity, fast kinetics governed by chemisorption, and optimal performance under mildly acidic to neutral conditions, which are relevant to many natural waters. While the material shows remarkable resilience against common anions like chloride and sulfate, its performance is competitively inhibited by phosphate and bicarbonate, a finding that mechanistically validates the ligand-exchange adsorption pathway and defines its suitable application scope. The successful regeneration over multiple cycles underscores the practical potential and cost-effectiveness of the adsorbent. Overall, this study provides a compelling strategy for stabilizing active phases on conductive supports and presents CaP-Cit@MWCNT as a promising candidate for advanced de-fluorination technologies, with clear pathways identified for future optimization and application in real-world scenarios.

CONFLICT OF INTEREST

The authors declare that there is no conflict of interests regarding the publication of this manuscript.

REFERENCES

1. Habuda-Stanić M, Ravančić M, Flanagan A. A Review on Adsorption of Fluoride from Aqueous Solution. Materials. 2014;7(9):6317-6366.
2. Chiavola A, D'Amato E, Di Marcantonio C. Comparison of Adsorptive Removal of Fluoride from Water by Different Adsorbents under Laboratory and Real Conditions. Water. 2022;14(9):1423.
3. Tolkou AK, Manousi N, Zachariadis GA, Katsoyiannis IA, Deliyanni EA. Recently Developed Adsorbing Materials for Fluoride Removal from Water and Fluoride Analytical Determination Techniques: A Review. Sustainability. 2021;13(13):7061.
4. Hashemkhani M, Rezvani Ghalhari M, Bashardoust P, Hosseini SS, Mesdaghinia A, Mahvi AH. Fluoride removal from aqueous solution via environmentally friendly adsorbent derived from seashell. Sci Rep. 2022;12(1).
5. Medellin-Castillo NA, Leyva-Ramos R, Ocampo-Perez R, Garcia de la Cruz RF, Aragon-Piña A, Martinez-Rosales JM, et al. Adsorption of Fluoride from Water Solution on Bone Char. Industrial and Engineering Chemistry Research. 2007;46(26):9205-9212.
6. Dionysopoulos D, Koliniotou-Koumpia E, Helvatzoglou-Antoniades M, Kotsanos N. Fluoride release and recharge abilities of contemporary fluoride-containing restorative materials and dental adhesives. Dent Mater J. 2013;32(2):296-304.
7. Burke FM, Ray NJ, McConnell RJ. Fluoride-containing restorative

materials. Int Dent J. 2006;56(1):33-43.
8. McCabe JF, Yan Z, Al Naimi OT, Mahmoud G, Rolland SL. Smart materials in dentistry. Aust Dent J. 2011;56(s1):3-10.
9. Tatevossian A. Distribution and kinetics of fluoride ions in the free aqueous and residual phases of human dental plaque. Arch Oral Biol. 1978;23(10):893-898.
10. Fan X. Adsorption kinetics of fluoride on low cost materials. Water Res. 2003;37(20):4929-4937.
11. Liang Z-S, Higuchi WI. Kinetics and mechanism of the reaction between hydroxyapatite and fluoride in aqueous acidic media. The Journal of Physical Chemistry. 1973;77(13):1704-1710.
12. Ebrahimi N, Soleimani AA, Rashidiani J, Malekafzali B, Abedini F, Hosseinkhani H. Chitosan/Fluoride Nanoparticles for Preventing Dental Caries. Current Dentistry. 2019;1(1):61-67.
13. Nguyen S, Escudero C, Sediqi N, Smistad G, Hiorth M. Fluoride loaded polymeric nanoparticles for dental delivery. Eur J Pharm Sci. 2017;104:326-334.
14. Kulshrestha S, Khan S, Hasan S, Khan ME, Misba L, Khan AU. Calcium fluoride nanoparticles induced suppression of Streptococcus mutans biofilm: an in vitro and in vivo approach. Applied Microbiology and Biotechnology. 2015;100(4):1901-1914.
15. Viana ÍEL, Lopes RM, Silva FRO, Lima NB, Aranha ACC, Feitosa S, et al. Novel fluoride and stannous -functionalized β-tricalcium phosphate nanoparticles for the management of dental erosion. J Dent. 2020;92:103263.
16. Patel G, Pal U, Menon S. Removal of Fluoride from Aqueous Solution by CaO Nanoparticles. Sep Sci Technol. 2009;44(12):2806-2826.
17. Hafshejani LD, Tangsir S, Daneshvar E, Maljanen M, Lähde A, Jokiniemi J, et al. Optimization of fluoride removal from aqueous solution by Al_2O_3 nanoparticles. J Mol Liq. 2017;238:254-262.
18. Dehghani MH, Haghighat GA, Yetilmezsoy K, McKay G, Heibati B, Tyagi I, et al. Adsorptive removal of fluoride from aqueous solution using single- and multi-walled carbon nanotubes. J Mol Liq. 2016;216:401-410.
19. Castro-Rojas MA, Vega-Cantu YI, Cordell GA, Rodriguez-Garcia A. Dental Applications of Carbon Nanotubes. Molecules. 2021;26(15):4423.
20. Nahorny S, Zanin H, Christino VA, Marciano FR, Lobo AO, Soares LES. Multi-walled carbon nanotubes/graphene oxide hybrid and nanohydroxyapatite composite: A novel coating to prevent dentin erosion. Materials Science and Engineering: C. 2017;79:199-208.
21. Ruan Z, Tian Y, Ruan J, Cui G, Iqbal K, Iqbal A, et al. Corrigendum to "Synthesis of hydroxyapatite/multi-walled carbon nanotubes for the removal of fluoride ions from solution" [Appl. Surf. Sci. 412 (2017) 578–590]. Appl Surf Sci. 2018;437:451-452.
22. Bhasin CP, Pathan A, Patel RV. An Evaluation of Carbon Nanotube-based and Activated Carbon-based Nanocomposites for Fluoride and Other Pollutant Removal from Water: A Review. Current Nanomaterials. 2024;9(1):16-40.
23. Ku Y, Chiou H-M. The Adsorption of Fluoride Ion from Aqueous Solution by Activated Alumina. Water, Air, and Soil Pollution. 2002;133(1-4):349-361.
24. Camacho LM, Torres A, Saha D, Deng S. Adsorption equilibrium and kinetics of fluoride on sol–gel-derived activated alumina adsorbents. Journal of Colloid and Interface Science. 2010;349(1):307-313.
25. Maliyekkal SM, Shukla S, Philip L, Nambi IM. Enhanced fluoride removal from drinking water by magnesia-amended activated alumina granules. Chem Eng J. 2008;140(1-3):183-192.
26. Tan TL, Krusnamurthy PAP, Nakajima H, Rashid SA. Adsorptive, kinetics and regeneration studies of fluoride removal from water using zirconium-based metal organic frameworks. RSC Advances. 2020;10(32):18740-18752.
27. Yan Y, Zhong Q, Wang Y, Lu K, Xia M, Luo H, et al. Facile construction of zirconium/iron bimetallic organic frameworks for fluoride efficient removal from aqueous phase: An integrated experimental and theoretical investigation. Journal of Colloid and Interface Science. 2025;681:376-391.
28. Belaye M, Taddesse AM, Teju E, Sanchez-Sanchez M, Yassin JM. Preparation and Adsorption Behavior of Ce(III)-MOF for Phosphate and Fluoride Ion Removal from Aqueous Solutions. ACS Omega. 2023;8(26):23860-23869.
29. Hou PX, Bai S, Yang QH, Liu C, Cheng HM. Multi-step purification of carbon nanotubes. Carbon. 2002;40(1):81-85.
30. Low KL, Tan SH, Zein SHS, McPhail DS, Boccaccini AR. Optimization of the mechanical properties of calcium phosphate/multi-walled carbon nanotubes/bovine serum albumin composites using response surface methodology. Materials and Design. 2011;32(6):3312-3319.
31. Yasmeen R, Islam SMS, Ayeni OM, Moghadam PZ, Du J, Omary MA. Effects of de-fluorination on hydrophobicity and on CO_2 and CH_4 adsorption under high humidity in MeMOFs, methylated analogues of FMOFs. Dalton Transactions. 2025;54(19):7641-7658.
32. Misra A, Tyagi PK, Singh MK, Misra DS. FTIR studies of nitrogen doped carbon nanotubes. Diamond Relat Mater. 2006;15(2-3):385-388.
33. Zhang W, Silva SRP. Raman and FT-IR studies on dye-assisted dispersion and flocculation of single walled carbon nanotubes. Spectrochimica Acta Part A: Molecular and Biomolecular Spectroscopy. 2010;77(1):175-178.
34. Saito T, Matsushige K, Tanaka K. Chemical treatment and modification of multi-walled carbon nanotubes. Physica B: Condensed Matter. 2002;323(1-4):280-283.
35. Gholami F, Zein SHS, Gerhardt L-C, Low KL, Tan SH, McPhail DS, et al. Cytocompatibility, bioactivity and mechanical strength of calcium phosphate cement reinforced with multi-walled carbon nanotubes and bovine serum albumin. Ceram Int. 2013;39(5):4975-4983.
36. Roguska A, Pisarek M, Andrzejczuk M, Dolata M, Lewandowska M, Janik-Czachor M. Characterization of a calcium phosphate–TiO_2 nanotube composite layer for biomedical applications. Materials Science and Engineering: C. 2011;31(5):906-914.
37. Khatkar R, Nagpal S. Defluorination Techniques: Past, Present and Future Prospective. Korean J Chem Eng. 2024;41(3):553-569.
38. Duffin S, Duffin M, Grootveld M. Revisiting Fluoride in the Twenty-First Century: Safety and Efficacy Considerations. Frontiers in Oral Health. 2022;3.
39. Mariappan Santhi V, Periasamy D, Perumal M, Sekar PM, Varatharajan V, Aravind D, et al. The Global Challenge of Fluoride Contamination: A Comprehensive Review of Removal Processes and Implications for Human Health and Ecosystems. Sustainability. 2024;16(24):11056.
40. Prasad ME, Karn SK, Singh P. Defluoridation by Microbes: A Potential Remediation Technique. Environmental Science and Engineering: Springer Nature Singapore; 2024. p. 193-221.